

# Safe and Compliant Control of Redundant Robots Using a Stack of Passive Task-Space Controllers

Carlo Tiseo<sup>1,\*</sup>, Wolfgang Merkt<sup>1,2,\*</sup>, Wouter Wolfsflag<sup>1</sup>, Sethu Vijayakumar<sup>1</sup>, and Michael Mistry<sup>1</sup>

**Abstract**—Safe and compliant control of dynamic systems in interaction with the environment, e.g., in shared workspaces, continues to represent a major challenge. Mismatches in the dynamic model of the robots, numerical singularities, and the intrinsic environmental unpredictability are all contributing factors. Online optimization of impedance controllers has recently shown great promise in addressing this challenge, however, their performance is not sufficiently robust to be deployed in challenging environments. This work proposes a compliant control method for redundant manipulators based on a stack of multiple passive task-space controllers. Our control framework of passive controllers is inherently stable, numerically well-conditioned (as no matrix inversions are required), and computationally inexpensive (as no optimization is used). We leverage and introduce a novel stiffness profile for a recently proposed passive controller with smooth transitions between the divergence and convergence phases making it particularly suitable when multiple passive controllers are combined in a stack. Our experimental results demonstrate that the proposed method achieves sub-centimeter tracking performance during dynamic demanding tasks with fast-changing references, while remaining safe to interact with and robust to singularities. The proposed framework achieves this without knowledge of the robot dynamics and thanks to its passivity is intrinsically stable. The data further shows that the robot can fully take advantage of the null-space to maintain the primary task accuracy while compensating for external perturbations.

## I. INTRODUCTION

Redundant robots—which have more Degrees of Freedom (DoF) than required for a task—have been widely studied and deployed due to their intrinsic flexibility. The higher dimensionality of the joint configuration space with respect to (w.r.t.) the task space makes these systems more adaptable as multiple solutions can be found. However, this flexibility introduces a higher complexity for both planning and control that rapidly increases with the system and task dimensionality. For example, computing the joint configuration from a task-space pose, i.e. inverse kinematics (IK), becomes increasingly more challenging with the increase of the redundancy dimension [1]. This problem is also encountered when dealing with the inverse dynamics problem, which is used to derive the control laws used in interaction control [1], [2]. To address these inverse problems in rigid systems, multiple optimization frameworks and approaches to deal

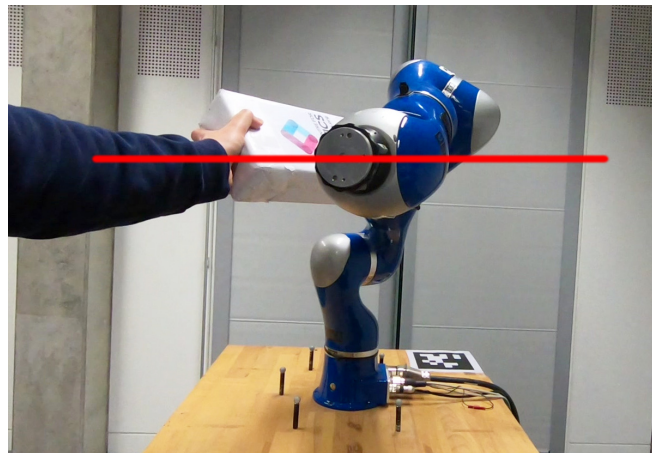


Fig. 1: Stack of Passive Controllers executing a reference motion to follow a line trajectory while an unknown external disturbance is introduced to the elbow joint. The controller adapts safely and compliantly to the disturbance and degrades tracking performance gracefully.

with challenges arising from numerical conditioning have been developed. Currently, inverse problems for soft robots<sup>1</sup> and dynamic task-space optimization are still open problems [2], [3].

### A. Inverse solutions for redundant systems

Inverse kinematics solutions and task-space dynamics projections are required for controlling redundant robots and they share similar challenges, as in depth analyzed in [4]. In summary, both problems rely on the inversion of the Jacobian matrix, which is non-square in redundant manipulator due to the different task and joint space dimensions [1]. The pseudo-inverse is a transformation that solves such problem. It separates the information regarding robot state in two orthogonal sub-spaces (task-space and null-space), which are not expected to exchange information (i.e., energy). Therefore, retaining the orthogonality between these two sub-spaces is paramount for the algorithms' stability [4]. Maintaining this orthogonality depends on both the robot kinematics and the task. Consequentially, it is extremely difficult to achieve and maintain, especially during highly variable situations, such as sudden changes in contacts and dynamic interactions (Figure 1). As one example, the dynamically consistent inverse obtains orthogonality via the minimization of the

\* The authors contributed equally to this work.

<sup>1</sup> Edinburgh Centre for Robotics, Institute of Perception Action and Behaviour, School of Informatics, University of Edinburgh, UK. Email: {ctiseo,wolfgang.merkt}@ed.ac.uk

<sup>2</sup> Oxford Robotics Institute, University of Oxford, UK.

This research is supported by the Engineering and Physical Sciences Research Council UK RAI Hub for Offshore Robotics for Certification of Assets (ORCA, grant reference EP/R026173/1) and European Union Horizon2020 project Memory of Motion (MEMMO, project ID: 780684).

<sup>1</sup>Here, we use soft robots to refer both to systems made from non-rigid materials as well as those with compliant control, e.g., collaborative robots.

kinetic energy projected by the null-space into the task-space [4], [5].

### B. Passive Controllers

Passive controllers have been proposed to theoretically guarantee interaction stability under uncertain interaction conditions, using for instance virtual tanks to mimic energy storage. However their passive behavior has been found difficult to realize in practice especially under highly variable dynamics [6]. Moreover, virtual tank impedance controllers are only passive if there is energy left in their virtual tanks. Due to passivity constraints, the tanks' energy can be only charged from external energy sources [6]. Realising passive control is made even more difficult when dealing with null-space and task-space controllers. In fact, as they are orthogonal to each other, tracking the total energy exchanged by the manipulator is challenging [7]. Another challenge to stability of virtual tank controllers is maintaining the orthogonality between null-space and task-spaces during highly variable tasks. Higher nonlinearity in the dynamics reduces the accuracy in the computation of the orthogonal projection that, consequentially, generates unaccounted energy transfer between the two sub-spaces [4], [7].

### C. Contribution

This work investigates the possibility of using a stack of task-space controllers to drive both task and null spaces, cf. Figure 2. Conceptually, this follows the idea to generate task-space wrenches at multiple links and map them back to joint-level torques. To do so the proposed solution will not need to rely on any mathematical projections (and implicitly, matrix inversions) to evaluate the null-space. Virtual mechanical constraints are instead generated using a stack of task-space controllers to control task-space and null-space in redundant manipulators. However, implementing such solution will require a controller framework that is intrinsically stable. The recently proposed Fractal Impedance Controller (FIC) [7] is a passive controller meeting this requirement. It relies upon a nonlinear stiffness behavior in the task-space to track the energy exchanged between the robot and the environment, and treats the unexpected energy flow from the null-space as an external perturbation. The controller uses the concept of fractal impedance for the implementation of a passive controller that can provide good performances in both trajectory and force tracking. Thereby it detaches the robot stability from the postural optimization, which are currently bounded for interaction controllers relying on quadratic programming (QP) optimization [2].

In summary, our contributions are:

- 1) Introduction of the concept of a *Stack of Passive Task-Space Controllers*, which can preserve a primary task by sacrificing secondary tasks to take advantage of the redundancy. As the framework only relies on the forward computation of kinematics and Jacobian, it is numerically stable and computationally inexpensive. Further, it can be used with uncertain and imprecise

dynamics models as it only relies on the kinematics model (II-D).

- 2) Proposal of a new force profile for a Fractal Attractor which enables a smooth transition between convergence and divergence phases (II-C).
- 3) Validation of our approach both in simulation to test contact interaction with unknown obstacles and in real hardware experiments (III) to evaluate reference tracking performance for fast reference motion (IV). As all open parameters have a physically tractable meaning and the controller is intrinsically stable, online tuning can safely be performed.

We will open source our implementation for simulation and hardware experiments with publication of this manuscript.

## II. METHOD

### A. Inverse Problem and Kineto-Static Duality

The generalized inverse of  $A \in \mathbb{R}^{n \times m}$  is defined as any matrix  $G \in \mathbb{R}^{m \times n}$  that satisfies the following equations:

$$\begin{cases} \vec{a} = G\vec{b} + (I_n - GA)\vec{a}_\epsilon = G\vec{b} + P\vec{a}_\epsilon \\ AGA - A = 0 \end{cases} \quad (1)$$

where  $\vec{a} \in \mathbb{R}^n$ ,  $\vec{b} \in \mathbb{R}^m$ ,  $\vec{a}_\epsilon \in \mathbb{R}^n$  and  $I_n \in \mathbb{R}^{n \times n}$  is the identity matrix.  $P$  is a projection matrix that projects a generic vector  $a_\epsilon$  into the null-space of  $A$ ,  $\mathcal{N}(A)$ . Redundant robots are more flexible than non-redundant systems, however, they do not have a bijective transformation between generalized coordinates and task-space. Thus, control algorithms rely on numerical optimization to solve the inverse problem and identify viable strategies. This is task dependent and degenerates when  $A$  drops rank (i.e.,  $\det(A) = 0$ ) [4], [2]. Specifically, the rank of the inverse projection matrix drops if the robot is in a singular configuration or the task constraints are violated (e.g., unexpected sudden loss of contact) [4].

The idea of taking advantage of the kineto-static duality to address the inverse problem has been introduced with the concept of Port-Hamiltonian control in [8], [9]. In fact, the kinematic joint-space information can be used to derive task-space behavior and task-space force interaction can be used to relate back to joint-space torques:

$$\begin{cases} \dot{\vec{x}} = J\dot{\vec{q}} \\ \vec{\tau} = J^T\vec{h} \end{cases} \quad (2)$$

where  $J \in \mathbb{R}^{n \times m}$  is the geometric Jacobian matrix,  $\vec{x} \in \mathbb{R}^n$  is the end-effector twist,  $\dot{\vec{q}} \in \mathbb{R}^m$  is the joint velocities' vector and  $\vec{h} \in \mathbb{R}^n$  is the end-effector wrench,  $\vec{\tau} \in \mathbb{R}^m$  is the joint torques' vector.

### B. Fractal Impedance Controller

A Fractal Impedance Controller controls the robot as an equivalent mass-spring system:

$$\Lambda_c(\vec{q})\vec{\ddot{x}} + K(\vec{x})\vec{x} = 0$$

where  $\Lambda_c(\vec{q})$  is the projection of the inertia matrix in the task-space. The state dependent stiffness gain ( $K(\vec{x})$ ) is derived

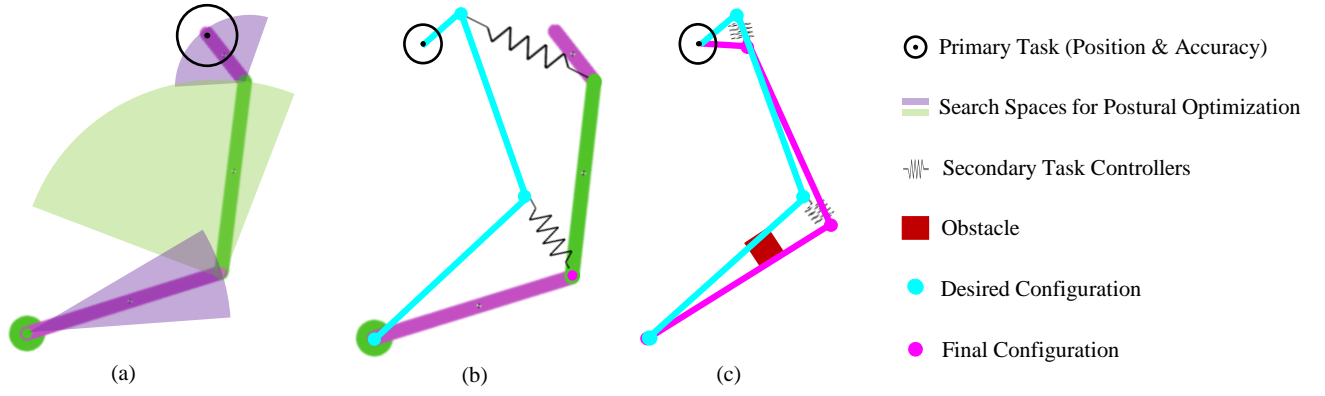


Fig. 2: Conceptual overview of the stack of passive task-space controllers framework: (a) The primary task is defined in terms of desired position, accuracy, and maximum exerted force produces a non-linear impedance profile to constrain the robot’s end-effector (3<sup>rd</sup>-link). Impedance profiles acting on additional links can subsequently be defined to control the robot joint-space configuration. Thus, the redundant manipulator is controlled via the interaction of several task-space controllers. (b) Exemplification of how the secondary tasks controllers pull the robot towards the desired configuration (c) In case an unknown obstacle is found on one of the links’ paths, the primary task controller guarantees that the end-effector gets as close as possible to the desired end-effector position despite the joint configuration converges to a different solution. Note, this adaptation is performed at the control level and does not involve replanning.

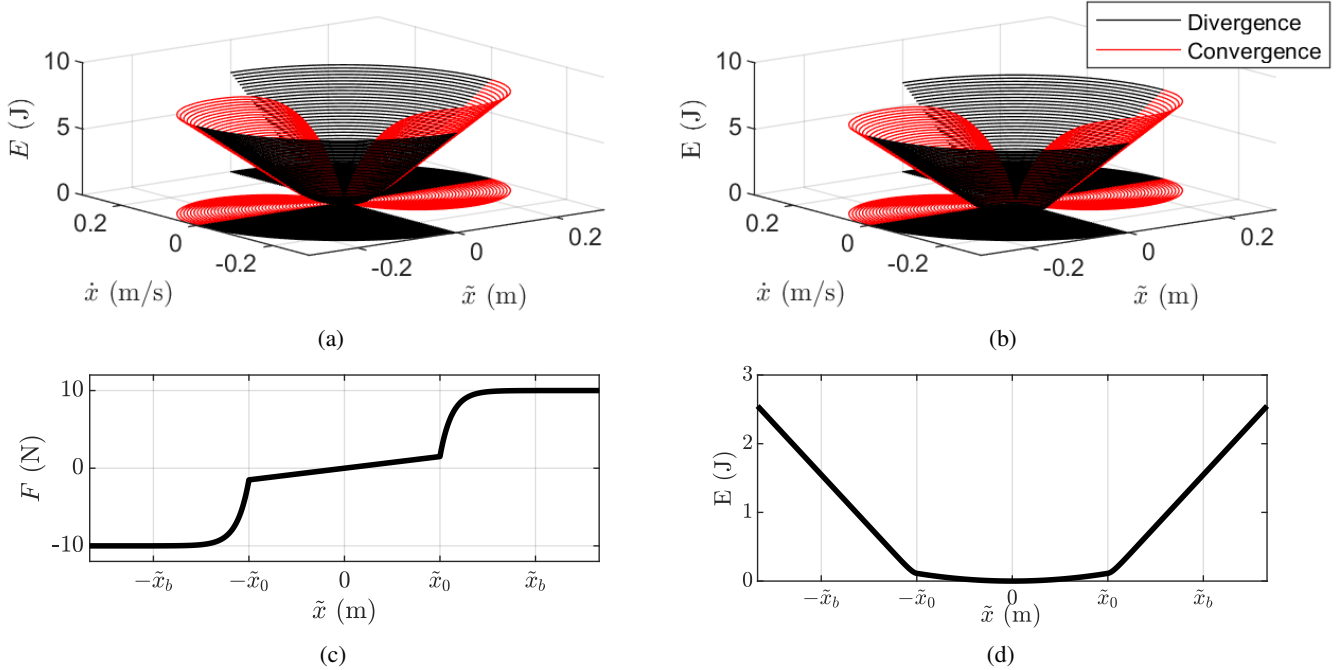


Fig. 3: (a) Fractal impedance attractor using a constant spring [7]. The trajectories beyond  $\tilde{x} > 0.3$  have been omitted (b) Fractal impedance attractor using the proposed spring (II-C), which differently from the linear spring has a compliant region near the fixed point in the desired state. The trajectories beyond  $\tilde{x} > 0.3$  have been omitted (c) Proposed force profile. (d) Energy profile associated with the proposed force profile.

from the desired end-effector interaction properties (i.e., force/displacement), which can be regulated online without affecting stability [7]. The attractor is implemented using a switching behavior that introduces an additional nonlinear spring which triggers when the system starts converging (i.e., zero crossing of  $\dot{\tilde{x}}$ ). The updated impedance conserves the energy accumulated in the controller while diverging and redistributes the energy altering the trajectory during the

convergence, as shown in Figure 3. Therefore, the stability of the controller is guaranteed by the fractal attractor (Figure 3). This determines the passivity of the controller and the online adaptability; it is independent of the chosen impedance.

For each DoF in the task-space, the FIC is given in algorithm 1. The control torques ( $\vec{\tau}_{ctr}$ ) can be calculated from  $\vec{h}_e \in \mathbb{R}^6$  using (2). Two limitations of the FIC control scheme introduced in [7] are (a) the inconsistency of the force

interaction when switching from divergence to convergence phase, and (b) the sharp saturation of the force profile. We will address both in the subsequent section.

---

**Algorithm 1:** Mono-dimensional FIC

---

**input :** Convergence/Divergence,  $\tilde{x}$ ,  $\tilde{x}_{\max}$

**output:**  $h_e$

1 **if** diverging from  $x_d$  **then**

2 |  $h_e = f(\tilde{x}) = K(\tilde{x})\tilde{x}$

3 **else**

4 |  $h_e = \frac{4E(\tilde{x}_{\max})}{\tilde{x}_{\max}^2}(0.5\tilde{x}_{\max} - \tilde{x})$

5 **end**

where:

$x_d$  is the desired position

$h_e$  is the desired force at the end-effector

$\tilde{x}$  is the pose error

$K(\tilde{x})$  is the nonlinear stiffness

$x_e$  is the end-effector position

$\tilde{x} = x_d - x_e$  is the position error

$\tilde{x}_{\max}$  is the maximum displacement reached at the end of the divergence phase

$E$  is the energy associated with the divergence profile of the impedance controller

---

### C. Sigmoidal Force Profile for Fractal Impedance

The FIC relies on a stiffness profile. The profile proposed in [7] results in fast changes in stiffness, and only allows limited task-dependent tuning of the profile. Therefore, we propose a sigmoidal force profile for an easier definition of the stiffness profile, allowing to better adapt the robot impedance behavior to the different task. Similarly to the profile proposed by [7], the sigmoidal profile is fully determined based on the maximum force ( $F_{\text{Max}}$ ) to be exerted at a chosen position error ( $|\tilde{x}| = \tilde{x}_b$ ). Here, the position error is defined as the difference between the desired end-effector pose and the current pose ( $\tilde{x} = x_d - x$ ). We introduce an additional displacement parameter ( $|\tilde{x}| = \tilde{x}_0$ ) which describes the minimum displacement to activate the nonlinear impedance, as shown in Figure 3c. The proposed force profile thus becomes:

$$F_K = \begin{cases} K_0\tilde{x}, & |\tilde{x}| < \tilde{x}_0 \\ \text{sgn}(\tilde{x})(1 - e^{-\frac{|\tilde{x}|-\tilde{x}_0}{b}}) + K_0\tilde{x}_0, & \tilde{x}_0 \leq |\tilde{x}| < \tilde{x}_b \\ F_{\text{Max}}, & \text{Otherwise} \end{cases} \quad (3)$$

where  $b = (\tilde{x}_b - \tilde{x}_0)/S$  is the characteristic length, and  $S$  determines the shape of the sigmoid curve. In this work, we use  $S = 20$  to ensure force saturation before  $\tilde{x}_b$ .

The proposed force profile can further be associated to an energy (Figure 3d) that is an unbounded Lipschitz function. It therefore respects the requirement for Lyapunov's stability by the fractal attractor controller [7]. For the proposed force

profile, this becomes:

$$E_K = \begin{cases} 0.5K_0\tilde{x}^2, & |\tilde{x}| < \tilde{x}_0 \\ F_{\text{Max}}|\tilde{x}| - F_{\text{Max}}\tilde{x}_0 + (K_0\tilde{x}_0^2)/2 - (1 - e^{-\frac{|\tilde{x}|-\tilde{x}_0}{b}})b\Delta F, & \tilde{x}_0 \leq |\tilde{x}| < \tilde{x}_b \\ F_{\text{Max}}|\tilde{x}| - F_{\text{Max}}\tilde{x}_0 + (K_0\tilde{x}_0^2)/2 - (1 - e^{-\frac{\tilde{x}_b-\tilde{x}_0}{b}})b\Delta F, & \text{Otherwise} \end{cases} \quad (4)$$

where  $\Delta F = (F_{\text{Max}} - K_0\tilde{x}_0)$ .

### D. Controller Stack for Null-Space Control

Null-space controllers can be seen as a way to handle redundancies via the introduction of optimization-based constraints to extra-dimensionality available in the joint-space of a redundant manipulator. Here, we propose to implement the same solution using virtual mechanical constraints generated by a stack of task-space controllers that drives the robot to assume a commanded reference posture. The benefit of using impedance controllers based on fractal impedance is that their passivity allows to stack them without compromising the system stability. Therefore, the total torque vector ( $\vec{\tau}_{\text{tot}}$ ) can be computed by the stack of controllers as:

$$\vec{\tau}_{\text{tot}} = \sum_{i=1}^n J_i^T h_{ei} \quad (5)$$

where  $J_i$  and  $h_{ei}$  are the Jacobian and the wrench generated by the impedance controller of the  $i^{\text{th}}$ -link, as depicted in Figure 2b and Figure 2c.

## III. EVALUATION

We evaluate our proposed method using a 7-DoF torque-controlled Kuka LWR3+ manipulator in both simulation and hardware experiments. We apply a stack of two task-space controllers: A 6-DoF FIC controller at the end-effector ( $7^{\text{th}}$  link) and a 3-DoF FIC controller at the elbow ( $3^{\text{rd}}$  link) for postural control. To generate pose references for each of the controllers in the stack, we perform an optimization to obtain a configuration satisfying the end-effector reference. Here, we use a one-step variant of Approximate Inference Control (AICO) [10]. Note, while the end-effector pose reference can be passed in directly to the end-effector controller, a postural optimization is used in this case to obtain a pose reference for the null-space or additional controllers in the stack. We extract the reference pose for each of the controllers using forward kinematics.

### A. Reference Trajectories

The figure-of-8 (i.e., lemniscate) trajectory has been designed to show the dynamic behavior of the robot. The trajectory is composed of two orthogonal sinusoidal trajectories. The vertical trajectory has an amplitude of 0.2 m and the transverse trajectory amplitude is 0.1 m. The figure-of-8 trajectory is particularly demanding due to its multiple velocity inversions and wide joint movements range. Thus,

	Simulations											
	Elbow Controller						End-Effector Controller					
	$x_0$ (m or rad)	.01	.01	.01	.057	.057	.057	.005	.005	.005	.057	.057
$x_b$ (m or rad)	.011	.011	.011	.63	.63	.63	.006	.006	.006	.63	.63	.63
$F_{Max}$ (N or N m)	50	50	50	0	0	0	150	150	150	100	100	100
$K_0$ (N m <sup>-1</sup> or N m rad <sup>-1</sup> )	5000	5000	5000	0	0	0	5000	5000	5000	100	100	100
	Robot											
	Elbow Controller						End-Effector Controller					
	$x_0$ (m or rad)	.01	.01	.01	.057	.057	.057	.06	.06	.06	.01	.01
$x_b$ (m or rad)	.011	.011	.011	.63	.63	.63	.08	.08	.08	.019	.019	.019
$F_{Max}$ (N or N m)	10	10	10	0	0	0	100	100	100	0	0	0
$K_0$ (N m <sup>-1</sup> or N m rad <sup>-1</sup> )	630	630	630	0	0	0	800	800	800	60	60	60

TABLE I: FIC Controller Parameters used for simulation and hardware experiments.

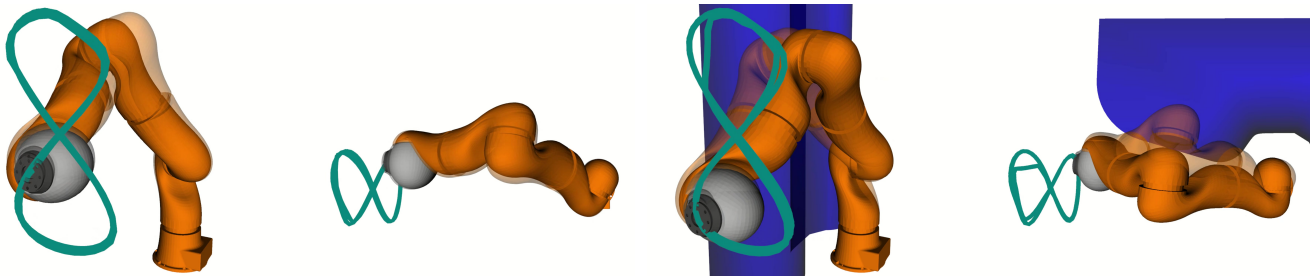


Fig. 4: Interaction with an unsensed object in simulation. The planned reference motion is shown with an alpha value while the real robot state is shown in solid, with the trace of the end-effector for both overlaid. Note, the controller remains in contact and follows the surface of the obstacle.

introducing high variability of both the Jacobian and the inertial behavior of the robot. We test the figure-of-8 reference motion in both simulation and hardware experiments.

In hardware experiments, we further test a sinusoidal trajectory with an amplitude of 0.5 m and velocities up to about 0.7 m s<sup>-1</sup>. The straight-line experiment enabled us to test interaction and robustness at higher speeds.

### B. Simulation Experiments

We simulate the robot using the Gazebo physics simulator and apply the Stack of Passive Task-Space Controllers control scheme directly without compensating for gravity, Coriolis, or other dynamic effects (in contrast to [7]), i.e., as a model-free compliant controller. For the simulation experiments, we compare nominal tracking performance with an interaction scenario where an unsensed environment obstacle has been introduced, cf. Figure 4.

### C. Hardware Experiments

In our hardware experiments, we use a Kuka LWR3+ robot. We control the manipulator using the Fast Research Interface (FRI) at 333.3 Hz in *joint impedance* mode with all gains set to zero to enable feed-forward torque control. Note, unlike our simulation experiments the Kuka’s built-in controller compensates for dynamic effects and gravity. On the real robot the tracking of the figure-of-8 trajectory has also been tested with and without a human operator applying random perturbations. The values used in the controller for the simulation and the experiments are reported in Table I.

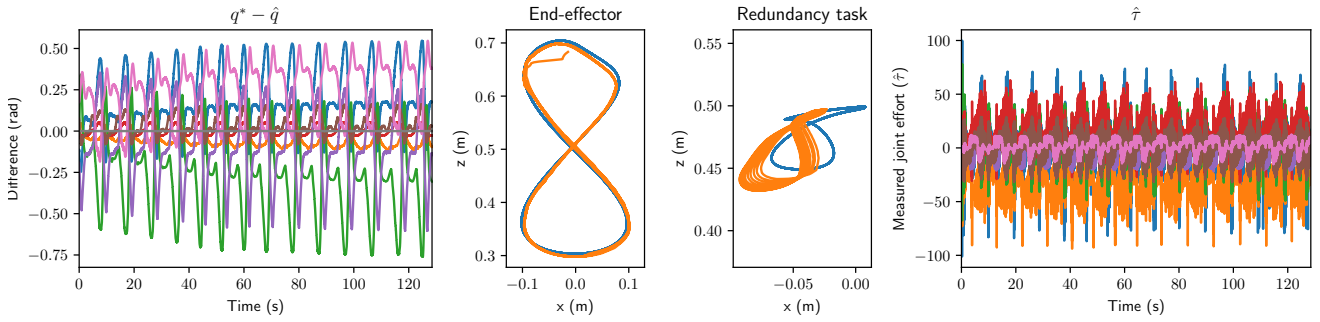
## IV. RESULTS

To complement the plots in this section, the reader is recommended to watch the supplementary video demonstrating the tracking and interaction both in simulation and hardware experiments. We also include a sequence demonstrating the safe behavior of the controller during calibration of the FIC parameters given in Table I.

The simulation results are shown in Figure 5 for the free motion, and in Figure 6 for the interaction behavior. They show that the robot can be successfully controlled without dynamic compensation, and that it can achieve dexterous dynamic behaviors. The tracking Root Mean Square Errors (RMSEs) at the end-effector are recorded without interaction as RMSE<sub>x</sub> = 5.6 mm, RMSE<sub>y</sub> = 4.6 mm, and RMSE<sub>z</sub> = 6.1 mm. For simulation with interaction with an obstacle: RMSE<sub>x</sub> = 13.2 mm, RMSE<sub>y</sub> = 4.2 mm, and RMSE<sub>z</sub> = 5.5 mm. I.e., the tracking performance degrades in one dimension impacted by the obstacle ( $x$ ), while being virtually unaffected in  $y$  and  $z$ .

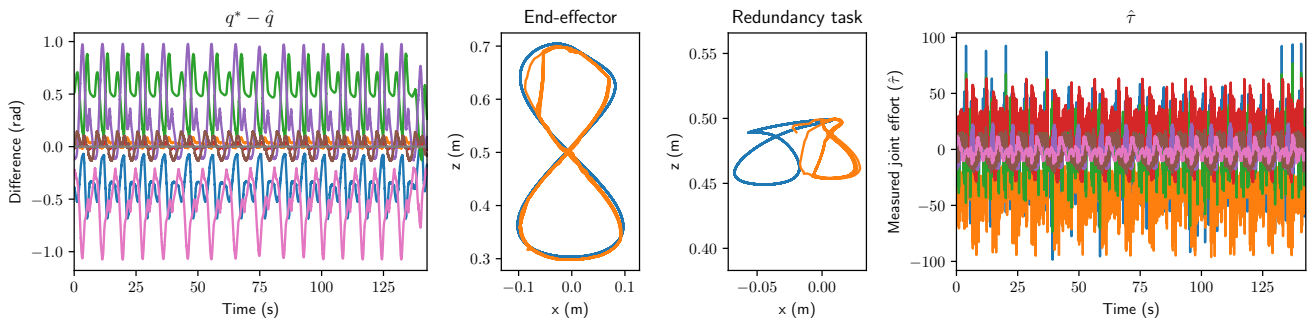
The experimental data for the hardware experiments of the figure-of-8 trajectory are shown in Figure 7 and Figure 8. The errors recorded during free motion are: RMSE<sub>x</sub> = 7.6 mm, RMSE<sub>y</sub> = 1.5 mm, and RMSE<sub>z</sub> = 8.6 mm. The perturbations do not affect the tracking performance at the end-effector task, but they are fully compensated by the deflection from the secondary task target at the elbow joint, as shown in Figure 8b. The RMSE during interaction are RMSE<sub>x</sub> = 20.3 mm, RMSE<sub>y</sub> = 7.9 mm, and RMSE<sub>z</sub> = 9.1 mm.

The results for the straight-line trajectory experiment (Figure 9 and Figure 10) show an ability of the controller



(a) Difference between reference motion and executed configuration (b) Task-space motion in  $xz$ -plane (reference in blue, executed in orange) (c) Measured joint space torques.

Fig. 5: *Simulation*: Fast figure-8, no interaction. Note, both the divergence in the joint position target (a) while closely tracking the end-effector reference (b). Further, as the simulation experiments are fully model-free, the torques are higher compared with Figure 7 as the FIC automatically compensates for gravity and dynamic effects.



(a) Difference between reference motion and executed configuration (b) Task-space motion in  $xz$ -plane (reference in blue, executed in orange) (c) Measured joint space torques.

Fig. 6: *Simulation*: Fast figure-8, interaction with unsensed obstacle (cf. Figure 4). The stack of passive task-space controllers compensates for the obstacle using the redundancy task by smoothly sliding across its surface, cf. (b). Note, that despite the interaction there are no torque spikes or instability, cf. (c).

to complete the task and reject perturbations by reducing tracking on the secondary task. The errors are  $\text{RMSE}_x = 6.1$  mm,  $\text{RMSE}_y = 4.6$  mm, and  $\text{RMSE}_z = 6.7$  mm. The RMSE for interaction are  $\text{RMSE}_x = 9.6$  mm,  $\text{RMSE}_y = 7.7$  mm, and  $\text{RMSE}_z = 7.3$  mm.

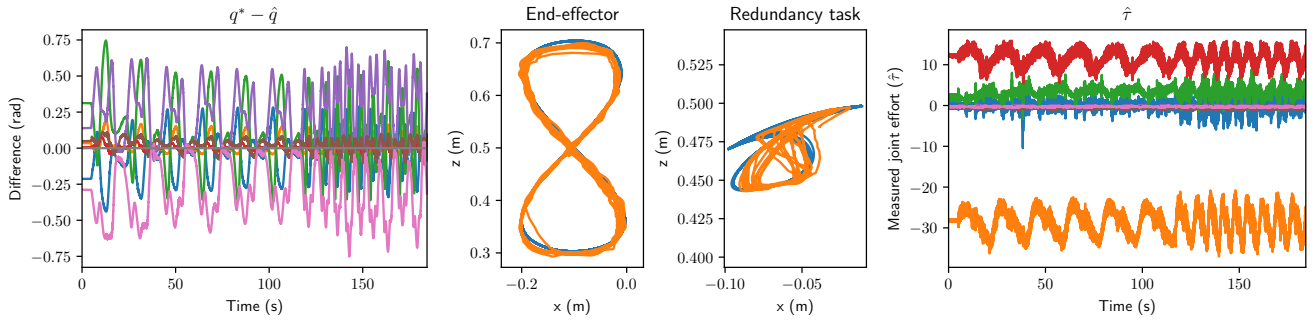
It shall also be remarked how the robot remained safe to interact with despite the high joint feed-forward torques involved in the motions, which reached  $\approx 30$  N m for both the 8 trajectory and the linear trajectory.

## V. DISCUSSION

The results show the proposed method makes it possible to generate an intrinsically stable control framework for redundant robots which does not rely on inverse dynamics and projection matrices. The method is robust to unknown environmental interactions and singularities. The data also confirm our hypothesis that redundant robots interaction behavior can be accurately defined without any *a priori* knowledge of the system dynamics model. In fact, our errors are on the same order of magnitude as the ones reported in [7], which included the robot dynamics compensation and null-space controller. This is particularly important because robots' mechanical properties such as Inertia and Joints

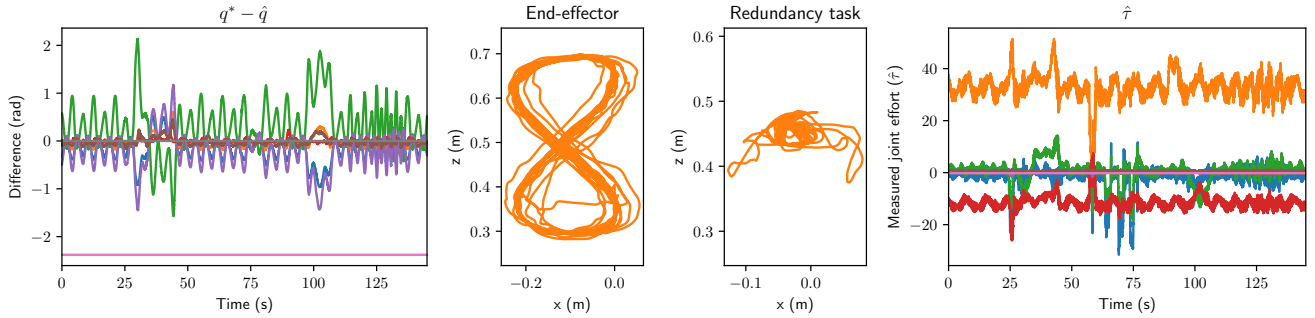
Friction matrices are often difficult to retrieve and highly unreliable [3], [11]. The knowledge of the actuation characteristics and the kinematic structure are still necessary for the implementation of the proposed method. However, they are both normally accurate, and easier to obtain if not available.

The stack of task-space controllers also opens new possibilities for improving controllability and dexterity for compliant robots, developing human motor control theory, and robust control architecture for learning algorithms. In fact, the dynamics of soft robots are even more challenging to model than rigid dynamics [3], as the dynamic modelling of robots is founded on the assumption of rigidity [1]. In regards to human motor control, having a framework that enables robustness and dexterity of interaction will enable to overcome the current limitation of the Passive Motion Paradigm (PMP) model, which still relies on inverse matrices for trajectory optimization [12], [13]. Finally, the learning algorithms are currently facing the challenges of performing a system identification to guarantee the stability of the learned behavior. The proposed method removes this challenge and the learning component can focus on learning how to synchronize the task-space controller to maximize the efficiency and the dexterity of the robot.



(a) Difference between reference motion and executed configuration (b) Task-space motion in  $xz$ -plane (reference in blue, executed in orange) (c) Measured joint space torques.

Fig. 7: *Hardware experiments: Fast figure-8, no interaction.* The controller tracks the reference closely both for the primary and redundancy tasks. Note, the divergence between reference configuration and accuracy of pose/posture tracking.



(a) Difference between reference motion and executed configuration (b) Task-space motion in  $xz$ -plane (reference in blue, executed in orange) (c) Measured joint space torques.

Fig. 8: *Hardware experiments: Fast figure-8, with interaction.* Note, the increase in measured joint efforts compared with Figure 7 due to the perturbations.

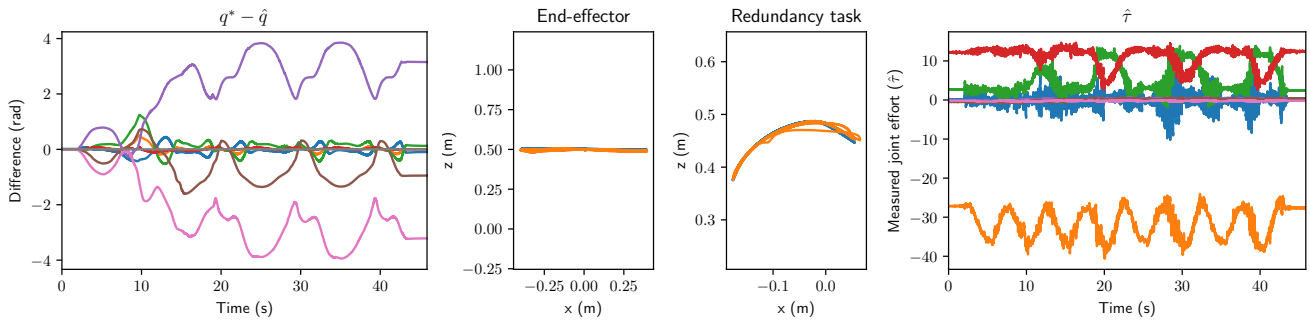
## VI. CONCLUSIONS

The experimental results confirmed our hypothesis that it is possible to control a redundant robot with a stack of task-space controllers. This approach renders the architecture intrinsically robust to singularity and fully passive which guarantees stability. It is important to properly balance the strength of the controllers to guarantee that the secondary tasks do not interfere with the end-effector controller, which may result challenging under certain conditions. Nevertheless, unbalanced controllers may interfere with the action efficacy but not with the robustness and stability of interaction.

This framework does not require any a priori knowledge of the system dynamics parameters (i.e., Inertia, Friction, and Gravity). It suited for applications where the stability of interaction to unpredictable environments is more important than the tracking accuracy. Future work will focus on improving the coordination among the secondary task-space controllers to improve the tracking accuracy of the end-effector task as well as systems were coupling effects may be introduced.

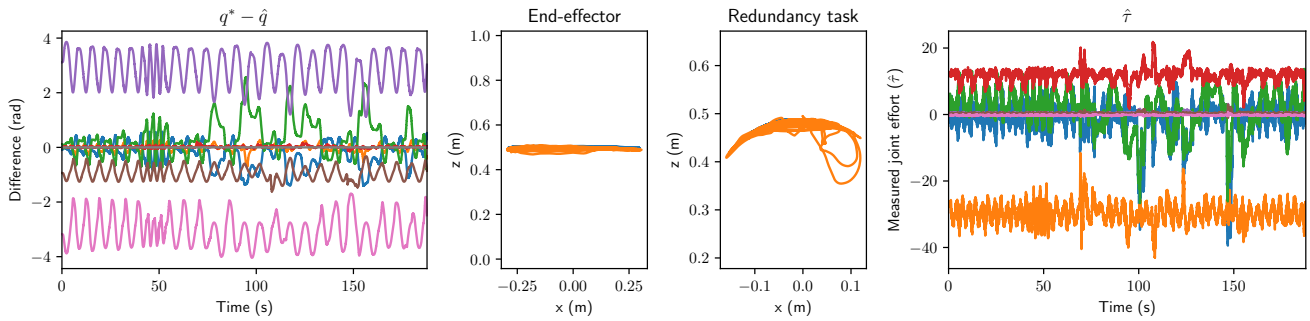
## REFERENCES

- [1] B. Siciliano, L. Sciacivco, L. Villani, and G. Oriolo, *Robotics: modelling, planning and control*. Springer Science & Business Media, 2010.
- [2] G. Xin, H. Lin, J. Smith, O. Cebe, and M. Mistry, “A model-based hierarchical controller for legged systems subject to external disturbances,” in *IEEE International Conference on Robotics and Automation (ICRA)*, May 2018, pp. 4375–4382.
- [3] D. Bruder, C. D. Remy, and R. Vasudevan, “Nonlinear system identification of soft robot dynamics using koopman operator theory,” in *IEEE International Conference on Robotics and Automation (ICRA)*, May 2019, pp. 6244–6250.
- [4] J. Moura, V. Ivan, M. S. Erden, and S. Vijayakumar, “Equivalence of the projected forward dynamics and the dynamically consistent inverse solution,” in *Proceedings of Robotics: Science and Systems*, Freiburg im Breisgau, Germany, June 2019.
- [5] O. Khatib, “A unified approach for motion and force control of robot manipulators: The operational space formulation,” *IEEE Journal on Robotics and Automation*, vol. 3, no. 1, pp. 43–53, 1987.
- [6] A. Dietrich, C. Ott, and S. Stramigioli, “Passivation of Projection-Based Null Space Compliance Control Via Energy Tanks,” *IEEE Robotics and Automation Letters*, vol. 1, no. 1, pp. 184–191, 2016.
- [7] K. K. Babarhamati, C. Tiseo, J. Smith, H. C. Lin, M. S. Erden, and M. Mistry, “Fractal impedance for passive controllers,” *arXiv preprint arXiv:1911.04788*, 2019.
- [8] N. Hogan, “Impedance control: An approach to manipulation: Part i – theory,” *Journal of dynamic systems, measurement, and control*, vol. 107, no. 1, pp. 1–7, 1985.
- [9] —, “Impedance control: An approach to manipulation: Part ii – implementation,” *Journal of dynamic systems, measurement, and control*, vol. 107, no. 1, pp. 8–16, 1985.
- [10] M. Toussaint, “Robot trajectory optimization using approximate inference,” in *International Conference on Machine Learning (ICML)*. ACM, 2009, pp. 1049–1056.
- [11] R. Vasudevan, “Hybrid system identification via switched system optimal control for bipedal robotic walking,” in *Robotics Research*.



(a) Difference between reference motion and executed configuration (b) Task-space motion in  $xz$ -plane (reference in blue, executed in orange) (c) Measured joint space torques.

Fig. 9: *Hardware experiments: Straight line reference, no interaction:* The robot tracks the task-space references for both the primary and redundancy task closely joint configurations are sacrificed.



(a) Difference between reference motion and executed configuration (b) Task-space motion in  $xz$ -plane (reference in blue, executed in orange) (c) Measured joint space torques.

Fig. 10: *Hardware experiments: Straight line reference ( $0.4 \text{ m s}^{-1}$  to  $0.7 \text{ m s}^{-1}$ ), with interaction:* Robot joint trajectories and effort during interaction experiments. The robot joints diverged significantly from the planned configuration, and reached position across singularities without any evident impact on the robot performance in terms of robustness and stability.

Springer, 2017, pp. 635–650.

- [12] P. Tommasino and D. Campolo, “An extended passive motion paradigm for human-like posture and movement planning in redundant manipulators,” *Frontiers in neurorobotics*, vol. 11, p. 65, 2017.
- [13] C. Tiseo, K. Veluvolu, and W. Ang, “The bipedal saddle space: modelling and validation,” *Bioinspiration & biomimetics*, vol. 14, no. 1, p. 015001, 2018.